Remote Sensing of Environment 152 (2014) 345–355

Contents lists available at ScienceDirect

Remote Sensing of Environment

journal homepage: www.elsevier.com/locate/rse

The scale-dependence of SMOS soil moisture accuracy and its improvement through land data assimilation in the central Tibetan Plateau

Long Zhao [a,b,c,*], Kun Yang [a], Jun Qin [a], Yingying Chen [a], Wenjun Tang [a], Hui Lu [d], Zong-Liang Yang [b]

[a] Key Laboratory of Tibetan Environment Changes and Land Surface Processes, Institute of Tibetan Plateau Research, Chinese Academy of Sciences, Beijing 100101, China
[b] Department of Geological Sciences, The John A. and Katherine G. Jackson School of Geosciences, The University of Texas at Austin, C1100 Austin, TX 78712–0254, USA
[c] University of Chinese Academy of Sciences, Beijing 100049, China
[d] Ministry of Education Key Laboratory for Earth System Modeling, and Center for Earth System Science, Tsinghua University, Beijing 100084, China

ARTICLE INFO

Article history:
Received 15 February 2014
Received in revised form 9 July 2014
Accepted 12 July 2014
Available online xxxx

Keywords:
SMOS
Soil moisture
Scale-dependence
Land data assimilation
Ground truth
Tibetan Plateau

ABSTRACT

This study evaluates SMOS (soil moisture and ocean salinity) soil moisture products against a newly established soil moisture network in the central Tibetan Plateau. Based on the results, the validity of assimilating the SMOS soil moisture retrievals into a land surface model is further evaluated. The ground truth is obtained by spatial upscaling from the network measurements within an area of approximately 10,000 km^2. Results show that both SMOS L2 and the preliminary version of L3 soil moisture products have large biases at the SMOS node scales (15 and 25 km), but they can reflect the surface wetness conditions well when averaged at a 100-km scale during the unfrozen season (June to October). This finding indicates the applicability of SMOS retrievals is scale-dependent. Meanwhile, very few retrievals are available in winter due to the presence of frozen soil and snow cover, and the accuracy of ascending retrievals degrades during transition when diurnal freezing–thawing cycle occurs. Considering the SMOS L2 product has a better accuracy than that of L3, we assimilate it into a land surface model using a dual-pass land data assimilation scheme. The data assimilation estimate without in-situ tuning proves superior to either remote sensing or land surface modeling in estimating surface soil moisture for the unfrozen season, and its accuracy fulfills the SMOS measurement requirements (RMSD ≤ 0.04 m^3 m^{-3}). Thus, the assimilation of SMOS retrievals holds promise to produce regional soil moisture dataset with acceptable accuracy for the Tibetan Plateau semi-arid region.

1. Introduction

As a critical component in the terrestrial water cycle, soil moisture controls a variety of the hydro-meteorological and biogeochemical processes, which is even more evident in semiarid areas where strong coupling between soil moisture and precipitation occurs (Koster et al., 2004). Microwave remote sensing (Bartalis et al., 2007; Kerr et al., 2001; Njoku, Jackson, Lakshmi, Chan, & Nghiem, 2003) and land surface modeling (Entin et al., 1999; Henderson-Sellers, Yang, & Dickinson, 1993) are possible ways to obtain surface soil moisture (SSM) at regional or global scales. However, the accuracy of microwave satellite product is often not satisfactory for many research and application purposes (Chen et al., 2013; dall'Amico, Schlenz, Loew, & Mauser, 2012). Meanwhile, the SSM estimated by land surface modeling strongly depends on the model structure and parameters as well as the accuracy of input forcing data (Henderson-Sellers et al., 1993).

It is commonly recognized that the low-frequency microwave emissions are highly related to SSM (Njoku & Entekhabi, 1996; Schmugge, 1978). For the past decades, various SSM products have been developed with the launch of several microwave sensors, such as AMSR-E (Advanced Microwave Scanning Radiometer for Earth Observing System) (Koike et al., 2004; Njoku & Chan, 2006; Owe, de Jeu, & Holmes, 2008) and ASCAT (METOP-A Advanced Scatterometer) (Bartalis et al., 2007). The newly launched SMOS satellite works at L-band (1.4 GHz) which is considered ideal for retrieving SSM (Kerr et al., 2001). Prior to this mission and up to present, several validations of SMOS SSM against intensive ground measurements have been conducted and obtained different biases, with most of them beyond the anticipation of the mission (Al Bitar et al., 2012; Albergel et al., 2012; dall'Amico et al., 2012; Dente, Su, & Wen, 2012; Gherboudj et al., 2012; Pan et al., 2012; Sanchez, Martinez-Fernandez, Scaini, & Perez-Gutierrez, 2012). The aforementioned evaluations are mainly conducted in Europe (Albergel et al., 2012; dall'Amico et al., 2012; Dente et al., 2012; Sanchez et al., 2012) and North America (Al Bitar et al., 2012; Gherboudj et al., 2012;

* Corresponding author at: Department of Geological Sciences, The John A. and Katherine G. Jackson School of Geosciences, The University of Texas at Austin, C1100 Austin, TX 78712–0254, USA.
E-mail address: zhaol04@gmail.com (L. Zhao).

http://dx.doi.org/10.1016/j.rse.2014.07.005
0034-4257/

Jackson et al., 2012; Pan et al., 2012). Yet, two major issues remain to be considered for further evaluation and utilization of SMOS SSM data.

The first one is about the spatial representativeness. The original spatial resolution of SMOS brightness temperature (TB) varies with incidence angles and has a nominal resolution of about 43 km. Taking the L2 data, for example, SSM is first obtained by minimizing the differences between observed and modeled TB at multi-viewing angles within a working area of 123 km × 123 km, and then oversampled to 15-km node scales (Kerr, Waldteufel, Richaume, et al., 2010). In previous evaluations, some simply conducted the node-to-site validation (Albergel et al., 2012), or averaged the closest in-situ point measurements within a SMOS node (dall'Amico et al., 2012; Gherboudj et al., 2012), and all found the SMOS data with large biases. However, Jackson et al. (2012) implemented evaluations at watershed scale by averaging both SMOS and in-situ measurements within a 600-km^2 area and found the SMOS data can approach the expected accuracy. Sanchez et al. (2012) considered different scale-matching strategies when evaluating SMOS L2 SSM data within a 1,300-km^2 area, and found the average-to-average (both SMOS L2 SSM and in-situ data are averaged in spatial) evaluation shows slightly better accuracy than at a single SMOS node scale. Nevertheless, in an even larger scale (40 km × 90 km), Dente et al. (2012) found the SMOS data failed in capturing the ground truth. Therefore, the impact of spatial scale on the oversampled L2 data still needs to be investigated in great detail.

The second issue is the low temporal resolution of SMOS SSM data (~3 days globally, if available). Due to the severe contamination of RFI at L-band (Oliva et al., 2012), SMOS retrievals are unavailable in quite a few regions over the world (Dente et al., 2012). A possible way to overcome this problem is by using land data assimilation, which is capable to take the advantage of continuous land surface model-output and make use of satellite observations (Crow & Wood, 2003; Houser et al., 1998; Li et al., 2007; Tian et al., 2009; Yang et al., 2007). In fact, great efforts have been made to directly assimilate the SMOS brightness temperature to estimate soil moisture within the framework of weather forecast (Kerr, Waldteufel, Wigneron, et al., 2010; Sabater, Fouilloux, & de Rosnay, 2011).

In this study, we evaluate the SMOS SSM data, investigate its scale-dependence, and conduct land data assimilation to explore the optimal utilization of SMOS soil moisture products for the Tibetan Plateau, where land–atmosphere interaction greatly impacts the energy and water cycle of the Asian monsoon system. We first evaluate the SMOS L2 and L3 SSM data within a newly established soil moisture network located in the central Tibetan Plateau. Evaluations at the SMOS node scale and at a coarser scale (~100 km) are conducted to study the scale-dependence of the SMOS product applicability. Then the selected SMOS SSM data are assimilated into a land surface model to achieve better temporal resolution and accuracy. Details about the network data, SMOS SSM data, and descriptions on evaluation strategy and the land data assimilation system are provided in Section 2. Evaluation and data assimilation results are presented in Section 3. Finally, all the analyses are summarized in Section 4.

2. Data and method

2.1. Ground data

The ground truth is collected within a recently established Central Tibetan Plateau Soil Moisture and Temperature Monitoring Network (CTP-SMTMN) within a spatial coverage of about 100 km × 100 km that matches a typical GCM (Global Climate Model) grid (Fig. 1a). This area has a generally slowly-varying terrain with rolling hills. Nearly 94% of the area is covered by alpine meadows, with very small water bodies at the west edge. High elevation and low temperature conditions are associated with very low biomass on the ground and less water vapor in the atmosphere, making this area an ideal place for microwave remote sensing of soil moisture. Besides, seasonal freezing–thawing processes are typical phenomenon within this area. The annual precipitation is approximately 400–500 mm, with three quarters during the monsoon season. Started from August 2010, the network was established through six field campaigns. Up to now, there are 56 stations in total (Fig. 1a shows the spatial distribution), each of which measures soil moisture and soil temperature at four layers (0–5 cm, 10 cm, 20 cm, and 40 cm). The ECH2O EC-TM/5TM probes are deployed, and the measured soil moisture data are calibrated to account for the impact of soil texture and organic carbon content. Note that the first layer soil moisture is measured by probes that are obliquely (approximately 45° slanted upward) inserted into the topsoil (0–5 cm). More details about the network construction and configuration can be found in Yang et al. (2013). This network is complementary to the existing Tibetan Plateau observatory that monitors plateau–scale soil moisture and soil temperature (Tibet-Obs) (Su et al., 2011). The data have been used to evaluate AMSR-E products and modeled soil moisture (Chen et al., 2013) and to analyze the spatiotemporal variability of soil moisture (Zhao, Yang, Qin, Chen, Tang, et al., 2013). The data are now available online (http://dam.itpcas.ac.cn/rs/?q=data) and archived in the database of the International Soil Moisture Network (Dorigo et al., 2011).

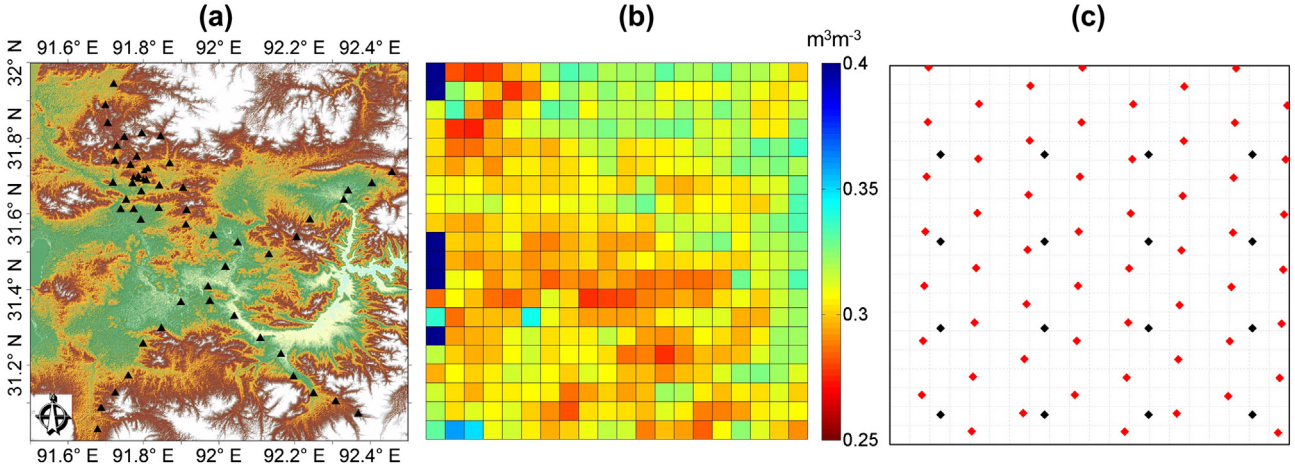

Fig. 1. (a) Spatial distribution of the CTP-SMTMN stations (black triangles). The base map shows the elevations. (b) Temporally averaged SSM for 2011 summer (June, July and August) that obtained through the upscaling with the aid of MODIS-observed apparent thermal inertia (ATI). (c) Spatial distribution of SMOS DGG nodes within the study area, where red and black diamonds denote the L2 (ISEA) and L3 (ESEA) node centers, respectively.

Because of the mismatch between a station and a satellite pixel, the upscaling of ground-based soil moisture observations is required (Crow et al., 2012). Based on the network measurements, Qin et al. (2013) developed a new upscaling scheme by introducing MODIS-derived apparent thermal inertia (ATI) as an extra data source to represent the SSM spatial variability. A function is first developed to link all station-averaged SSM and MODIS pixel-averaged ATI over the network, and then used to estimate SSM at finer scales. However, this pure ATI-based estimate may contain uncertainties because of the empirical function. Thus the final SSM estimate at a targeted scale is obtained by a weighted linear combination of station observations, and the weight numbers are optimized through Bayesian linear regression which minimizes the difference between the linear combination estimated and ATI-based SSMs. A demo for the Bayesian regression in the upscaling scheme is available online (http://dam.itpcas.ac.cn/rs/?q=prog). As an example, Fig. 1b shows the spatial variation of upscaled SSM with a 0.05° resolution (approximately 5 km). Note that there are several wetter cells at the western edge due to the existing of water bodies. In this study, the SSM estimated by the upscaling scheme is used as the ground truth.

2.2. SMOS data

Launched on November 2, 2009, the SMOS satellite was injected into a low-earth, polar sun-synchronous orbit at 750 km mean altitude. The onboard microwave radiometer deploys a Y-shaped antenna in compromising between the efficiency of soil moisture retrieving and the feasibility in engineering. According to its design, the microwave sensor can provide pixel brightness temperatures over different polarizations and multi-incidence angles (from 0° to 55°) across a 900-km swath. Generally the spatial resolution is within 30–50 km. The globe can be fully imaged twice every 3 days at 6:00 am (ascending) and 6:00 pm (descending) Local Solar Time (LST) (McMullan et al., 2008). The SMOS satellite provides L-band microwave brightness temperature, and it is expected to retrieve SSM with 0.04 $m^3\ m^{-3}$ accuracy over land (Kerr, Waldteufel, Wigneron, et al., 2010).

The SMOS group is now delivering two sets of SMOS SSM data, namely, the L2 and L3 soil moisture data that processed and delivered by ESA (European Space Agency) and CATDS (Centre Aval de Traitement des Données SMOS), respectively. Note that the L2 data are a mature product while the L3 data are currently a preliminary version and has just been released. For L2 data, as mentioned before, SSM and other surface variables are obtained by using an iterative scheme to minimize cost function that counts for the difference between model simulated and SMOS observed multi-angular TB data (Kerr et al., 2012). An L-band Microwave Emission of the Biosphere (L-MEB) model developed by Wigneron et al. (2007) is used to calculate brightness temperature based on initial SSM and auxiliary data in this process. The L3 SSM retrieval processor is based on the one developed in L2, with added ability on multi-orbit retrieving. This coherence between the ESA L2 and CATDS L3 processors makes it possible to take advantages of the two developments. Both two datasets use Discrete Global Grid (DGG) gridding system with a slight difference in projection. For ESA processors, it is the Icosahedral Snyder Equal Area Earth fixed grid (ISEA; ~15 km); for CATDS processors, it is the Equal-Area Scalable Earth Grid (EASE; 25 km). Comprehensive descriptions on the L2 and L3 soil moisture retrieval algorithm are provided in the ATBD document of Kerr, Waldteufel, Richaume, et al. (2010) and Kerr et al. (2013), respectively. The L2 operational data are available through EOLi-SA (http://earth.esa.int/EOLi/EOLi.html) and the L3 SSM data can be obtained from CATDS (http://catds.ifremer.fr/Products/Available-products-from-CPDC). In the CTP-SMTMN network, there are 56 and 16 of SMOS L2 and L3 grid nodes, respectively (see Fig. 1c for the spatial distribution of SMOS nodes).

To our knowledge, previous evaluations are mainly focused on the L2 data, and very few on the L3 data (Al-Yaari et al., 2014) due to the time lagging in data publicizing. In addition, the difference between ascending and descending retrievals remains unclear (Dente et al., 2012; Jackson et al., 2012; Rowlandson, Hornbuckle, Bramer, Patton, & Logsdon, 2012; Sanchez et al., 2012). Therefore, the SMOS L2 and L3 SSM data of both ascending and descending overpasses are investigated.

2.3. Evaluating SMOS retrieved SSM

For both SMOS L2 and L3 soil moisture products, the ascending and descending overpasses are assessed separately to investigate the possible influence of different temperature gradient within the topsoil on the retrieval algorithm. The analyzed period is from August 1, 2010 to October 1, 2012, including both frozen and non-frozen periods. Observed surface soil temperature and MODIS derived Snow Cover Fraction (SCF) data are jointly used to distinguish the snow cover and frozen conditions, as their existence may introduce additional uncertainties in SMOS soil moisture retrieving. Fig. 2 shows the observed hourly minimum surface soil temperature of all stations (LST_{min}) and Terra/Aqua satellite retrieved MODIS SCF (Hall, Salomonson, & Riggs, 2006a,b) within the CTP-SMTMN area. First, LST_{min} of 0 °C is used to approximately diagnose the soil frozen status. Second, considering part of the network area with extremely higher elevation may always have snow cover during the whole summer (Fig. 1a), SCF of 2% is used to indicate snow cover condition. Finally, based on criterions of $LST_{min} \geq 0$ °C and SCF < 2%, the period from June 1 to October 1 in both year 2011 and 2012 is identified to be unfrozen and snow-free (hereafter referred to as "unfrozen" period for simplicity), and the period beyond this unfrozen period is identified to be frozen or snow-covered (hereafter referred to as "frozen" period). Note that June 8, 2011 has SCF of 23%, yet there are no SSM retrievals within neither L2 nor L3 products at all SMOS nodes on this date, and thus the selected unfrozen period is still valid.

To investigate the scale-dependence of the accuracy of SMOS SSM products, we conducted two evaluations. The first is a node-to-average evaluation at SMOS node scale (15 km for SMOS L2 data and 25 km for L3 data). It compares the SMOS data with the ground truth of SSM derived from the algorithm of Qin et al. (2013) (Fig. 1b). The 5-km grids (shown in both Fig. 1b and c) are first assigned to a certain SMOS node by considering their distances to the node center, then a spatial average is made among grids that "belong to" the same SMOS node. The second evaluation is an average-to-average evaluation at a coarser scale (100 km). It is a comparison between average of all SMOS data and average of all the 5-km gridded SSM within this area. Each SMOS SSM at the node scale, including its average at the 100-km scale, is hereafter referred to as an "Effective Retrieval" (ER). The correlation coefficient (R), BIAS (SMOS retrievals minus upscaled in-situ SM), and root mean square difference (RMSD) are calculated as performance metrics to describe the evaluation results.

2.4. The dual-pass land data assimilation scheme

To improve the accuracy and overcome the low temporal resolution of SMOS retrievals, we assimilate the SMOS SSM data into a land surface model under the framework of the Dual-pass Land Data Assimilation Scheme of University of Tokyo (LDASUT) developed by Yang et al. (2007).

The essence of the LDASUT is the differentiating time scales used for the estimation of model parameters (%sand, %clay, and soil porosity) and state variables (SSM). Model parameters are usually time-invariant and have a long-term effect on model state variables, and thus they are estimated within a relatively long time window (months), which is so-called Pass 1 or optimization pass. By contrast, SSM changes rapidly with precipitation, and thus is estimated within a relatively short time window (1 day), which is so-called Pass 2 or assimilation pass. To apply this framework, a time-split approach is adopted. The flowchart for assimilating SMOS soil moisture product is shown in Fig. 3.

The model operator in this assimilation system is the Simple Biosphere scheme version 2 (SiB2) (Sellers et al., 1996), which has

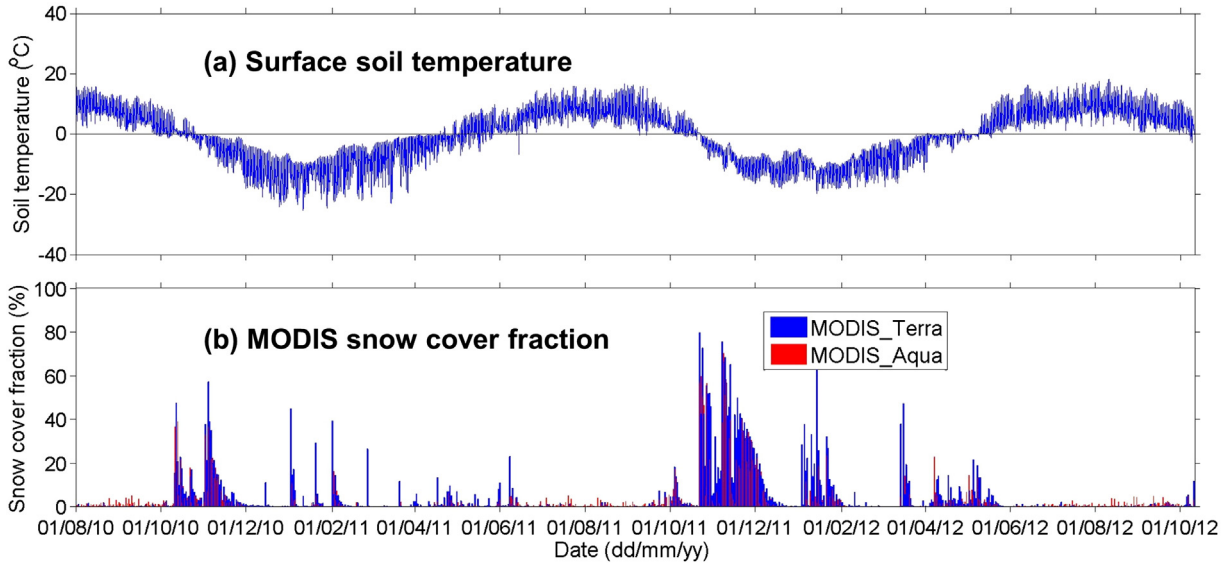

Fig. 2. (a) Observed hourly minimum surface soil temperature of all stations. (b) Spatially averaged time series of Terra and Aqua retrieved 0.05° MODIS snow fraction data within the soil moisture network area; note that only the data with "good" quality is used.

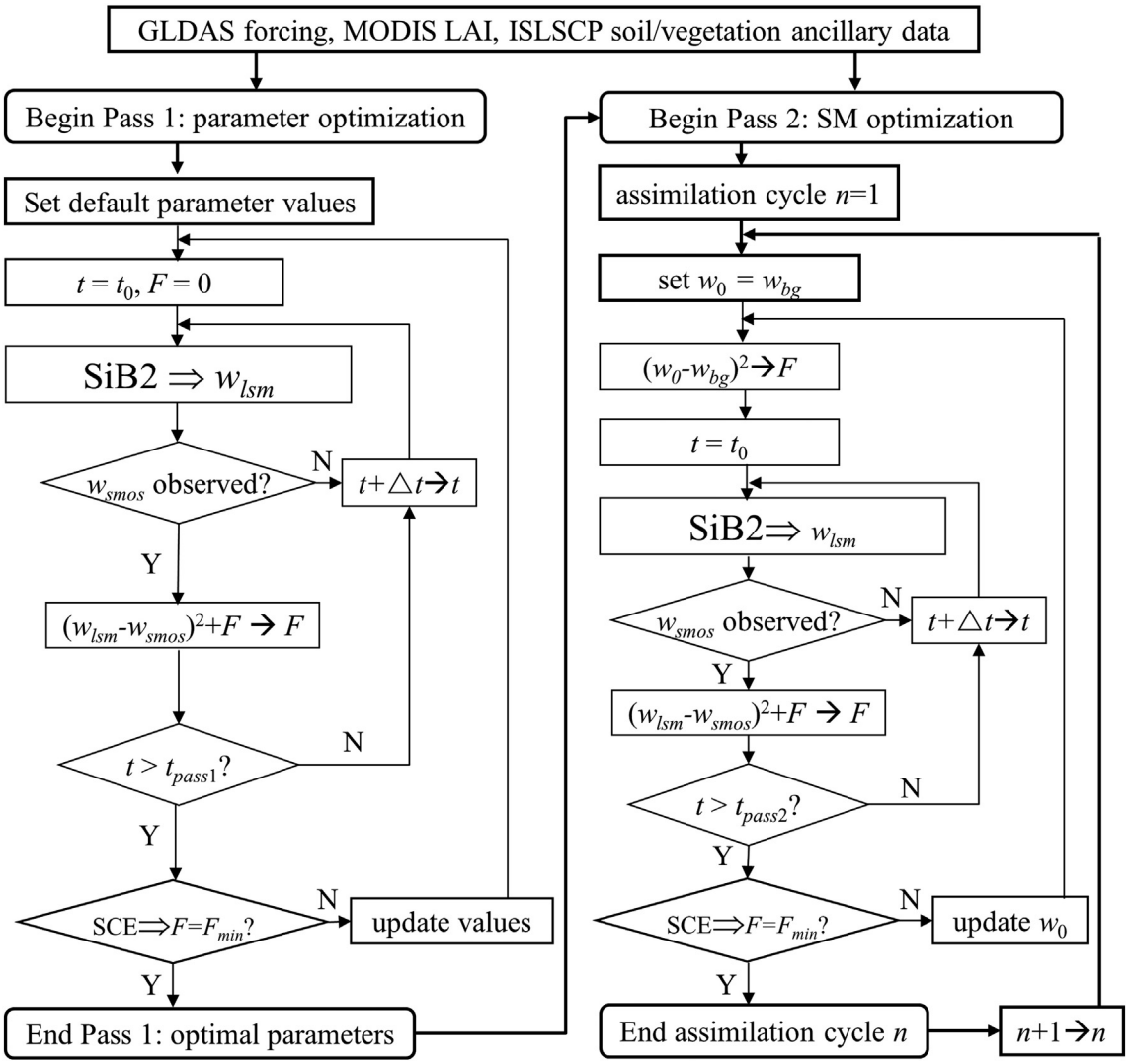

Fig. 3. Flowchart of the dual-pass scheme for assimilating SMOS soil moisture data.

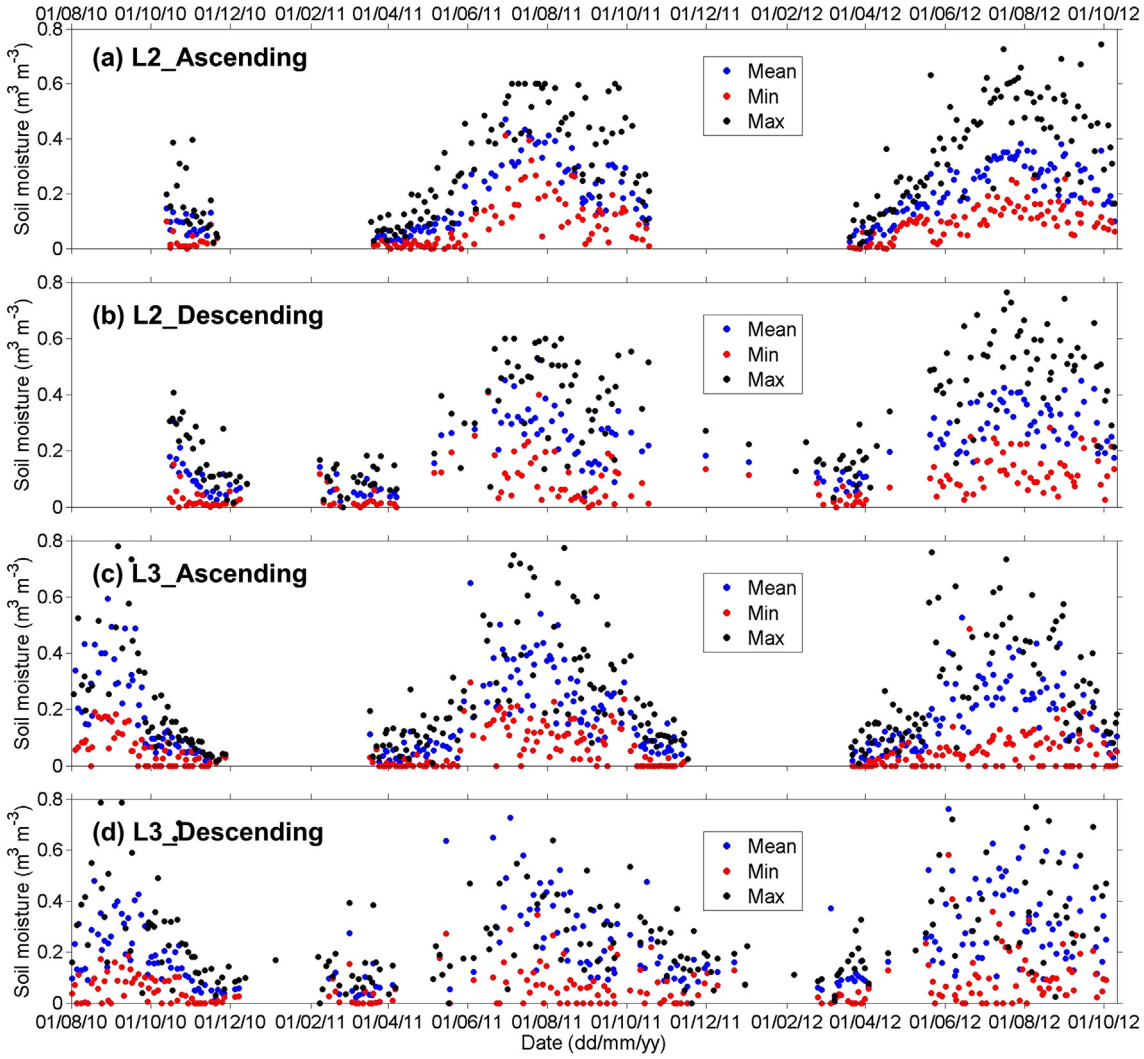

Fig. 4. Time series of mean, maximum, and minimum SSM among all SMOS nodes within the CTP-SMTMN area.

been revised to adapt the Tibetan Plateau environment (Yang et al., 2007). The thickness of surface soil layer in SiB2 is set to 5 cm to match the SMOS penetrating depth (first several cm). In addition, in each assimilation cycle, only surface soil moisture is updated. The soil moistures at deeper layers (root zone of 5–25 cm and recharge zone 25–150 cm) are impacted by the change of the topsoil moisture through soil water flow dynamics but are not directly modified by the assimilation. In both passes, the model operator is initialized with either default parameters (in Pass 1) or surface soil moisture (in Pass 2), and it simulates SSM at hourly time step with input forcing data and vegetation dynamic parameters. When SMOS retrieval is available, the difference between modeled and remotely sensed soil moisture is accumulated in a cost function. At the end of each assimilation window, a Shuffled Complex Evolution (SCE) approach (Duan, Gupta, & Sorooshian, 1993) is used to minimizing the cost function to find either the optimal model parameter values (in Pass 1) or initial soil moisture (in Pass 2). Specifically, in Pass 1, only soil clay content, sand content, and soil porosity are optimized. Other parameters (e.g., soil water retention parameters and hydraulic conductivity) are calculated from these optimized parameters based on empirical pedotransfer equations (see details in Yang et al., 2007). The optimized parameters in Pass 1 are then fed to Pass 2 for soil moisture optimization. In Pass 2, at the beginning of each assimilation cycle, soil moisture is initialized with the one inherited from last assimilation cycle and then updated through SCE. The difference between initial and updated soil moisture values further forms the background error term. The cost functions defined in the two passes are as follows:

$$\text{Pass 1} \quad F = \sum_{t=0}^{t_{pass1}} (w_{smos} - w_{lsm})^2 \tag{1}$$

$$\text{Pass 2} \quad F = \alpha \sum_{t=0}^{t_{pass2}} (w_{smos} - w_{lsm})^2 + (1-\alpha)\left(w_{bg} - w_0\right)^2 \tag{2}$$

where w_{smos} is SMOS retrieved SSM, and w_{lsm} is SiB2 simulated SSM at the SMOS observing time. w_{bg} is the initial background value at the beginning of each assimilation cycle, and w_0 is the renewed one after assimilating SMOS SSM. The first part in Eq. (2) is the observation error term and the second part is the background error term. Note that the background error term is only calculated once, while the observation error term is calculated every time when SMOS SSM is available in each assimilation cycle. α (0–1.0) is the weighting number to balance the two terms in Eq. (2). Since both the land surface model and satellite

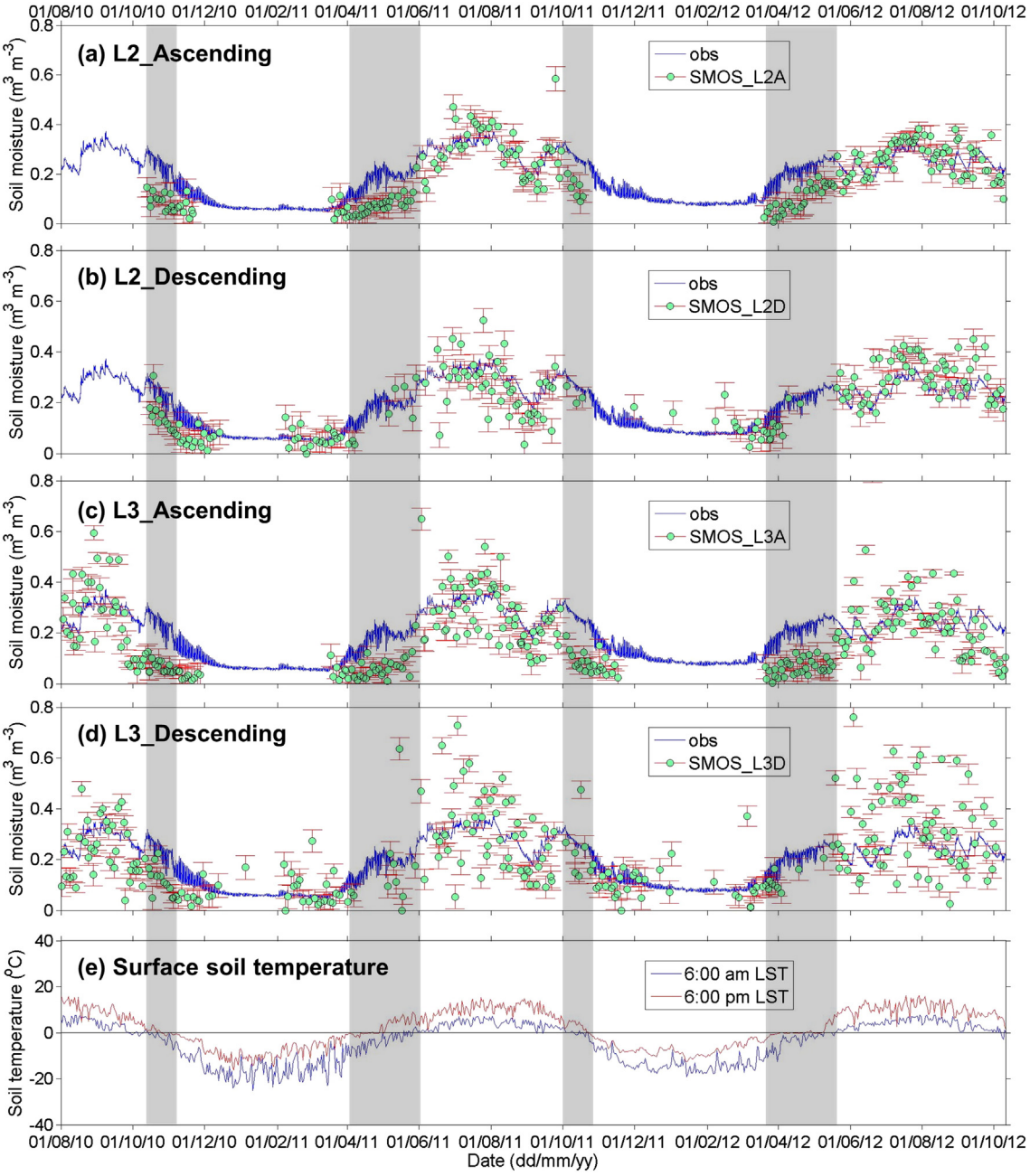

Fig. 5. (a) Time series of spatially averaged SMOS SSM retrievals (green dots: L2 ascending product) and ground truth (blue curve) at the 100-km scale, where the vertical range of the error bars are proportional to the number of SMOS nodes available for averaging. (b–d) Same as (a), but for SMOS L2 descending, L3 ascending, and L3 descending products, respectively. (e) Observed 6:00 am (blue) and 6:00 pm (red) minimum surface soil temperatures of all stations from August 1, 2010 to October 1, 2012.

Table 1
Evaluation results of SMOS L2 and L3 soil moisture products during unfrozen and snow-free period (from June 1st to October 1st in both year 2011 and 2012) within the CTP-SMTMN network.

Orbits	SMOS SM	Scale (km)	No.			*R*			BIAS			RMSD		
			Min	Max	Mean	Min	Max	Mean	Min	Max	Mean	Min	Max	Mean
Ascending	L2	15	2	98	47	−0.34	0.77	0.41	−0.102	0.060	−0.021	0.089	0.150	0.114
		100	/	/	103	/	/	0.68	/	/	0.012	/	/	0.060
	L3	25	31	152	97	−0.10	0.48	0.26	−0.144	0.031	−0.056	0.156	0.275	0.206
		100	/	/	122	/	/	0.30	/	/	−0.008	/	/	0.117
Descending	L2	15	1	70	27	−0.19	0.77	0.41	−0.150	0.106	0.005	0.081	0.179	0.133
		100	/	/	97	/	/	0.39	/	/	0.014	/	/	0.088
	L3	25	0	126	61	0.02	0.36	0.17	−0.111	0.108	0.027	0.199	0.311	0.260
		100	/	/	115	/	/	0.25	/	/	0.046	/	/	0.158

(No.: number of effective retrievals; units for BIAS and RMSD: $m^3\ m^{-3}$).

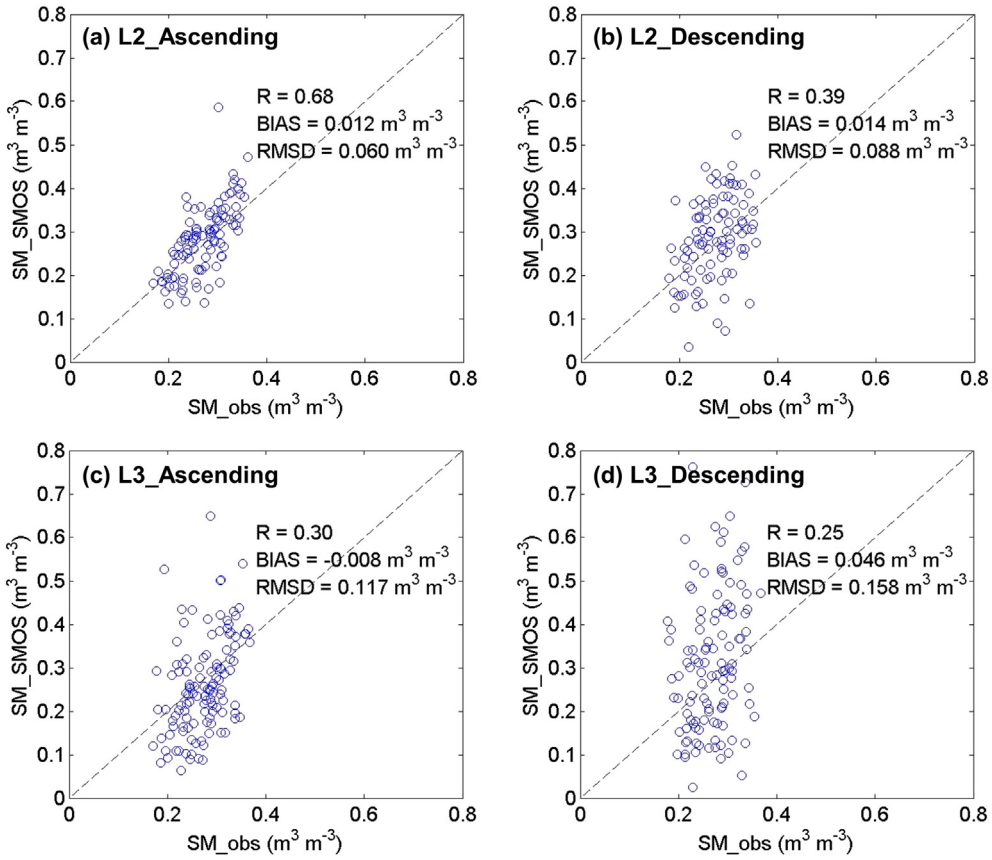

Fig. 6. Scatter plot between ground truth and spatially averaged SMOS SSM for the unfrozen and snow-free period (from June 1st to October 1st in both year 2011 and 2012).

observations may have errors, α can be considered to reflect error trade-off between these two error sources. The smaller value of α means the estimation of soil moisture will trust more on land surface model, and vice versa. Here we assign $\alpha = 0.5$ as the default value, and a sensitivity analysis in Section 3.3.1 will show its validity.

This dual-pass scheme is distinct from other methods that estimate state variables and parameters by state augmentation under the framework of Kalman filter (Young, 2002) and particle filter (Qin et al., 2009), or methods that deploy an ensemble of model replicates to represent the model uncertainties and errors through ensemble Kalman filter (Margulis, McLaughlin, Entekhabi, & Dunne, 2002; Pan & Wood, 2006). Meanwhile, the dual-pass concept used in this assimilation system also differs from the ones in which both parameters and state variables (Montzka et al., 2011; Moradkhani, Sorooshian, Gupta, & Houser, 2005) or both model and observation error parameters (Reichle, Crow, & Keppenne, 2008) are interactively estimated in an ensemble Kalman/particle filter-based sequential assimilation framework.

3. Result and discussion

3.1. SMOS Evaluation results

Fig. 4 shows the statistics of all SMOS retrievals at the node scale for the whole evaluation period. Generally, all retrievals show great spatial variations, and this is more evident for the descending overpass. Nevertheless, when averaged at a 100-km grid (Fig. 5a–d), the SMOS SSM data can follow the seasonal variations of ground truth much better. Meanwhile, there are fewer (for descending overpass; Fig. 4b and d) or even no (for ascending overpass; Fig. 4a and c) retrievals at all nodes during the winter when the topsoil became frozen and the land was occasionally covered by snow. This phenomenon is not surprising as it is still challenging to account for the impacts of snow cover and frozen soil in the soil moisture retrieval (Kerr, Waldteufel, Wigneron, et al., 2010).

An issue for the unfrozen season (from June 1st to October 1st in 2011 and 2012) is the shortage of ERs. To quantify the evaluation result, we counted the number of ERs for all nodes during the unfrozen season, and calculated the statistical indices (R, BIAS, and RMSD) against the ground truth when at least 10 ERs were available. Table 1 shows the minimum, maximum, and mean values of ERs, as well as the statistical metrics for both L2 and L3 retrievals. The evaluation results at the 100-km scale are also presented in Table 1 and Fig. 6. Several findings can be obtained, as follows.

First, the errors in the retrievals are scale-dependent. As mentioned before, the available ERs are limited during unfrozen periods. For instance, among all the 56 L2 SMOS nodes, the minimum and the maximum number of ERs are 2 and 98, respectively, with an average of 47. However, when averaged at the 100-km scale, the ER number increased up to 103. In terms of accuracy in capturing the ground truth, SMOS retrieval at the SMOS node scale has large biases, while it performs much better when averaged over the 100-km scale (i.e., the second evaluation) (see the higher correlation coefficient, smaller BIAS and RMSD values in Table 1 and Fig. 6). Particularly, RMSD values for L2 retrievals are over 0.100 $m^3\ m^{-3}$ in ascending overpass at a 15-km scale, but within 0.060 $m^3\ m^{-3}$ when averaged at the 100-km scale. The latter is much closer to the anticipated accuracy of SMOS mission (0.040 $m^3\ m^{-3}$). Similar results are obtained for all evaluations for both L2 and L3 data, and both overpasses, except for evaluation on SMOS L2 descending overpass, which obtained a correlation coefficient slightly lower at the 100-km scale ($R = 0.39$) than at the 15-km scale ($R = 0.41$). From this point of view, the SMOS retrievals can be directly used for large-scale drought monitoring for this region.

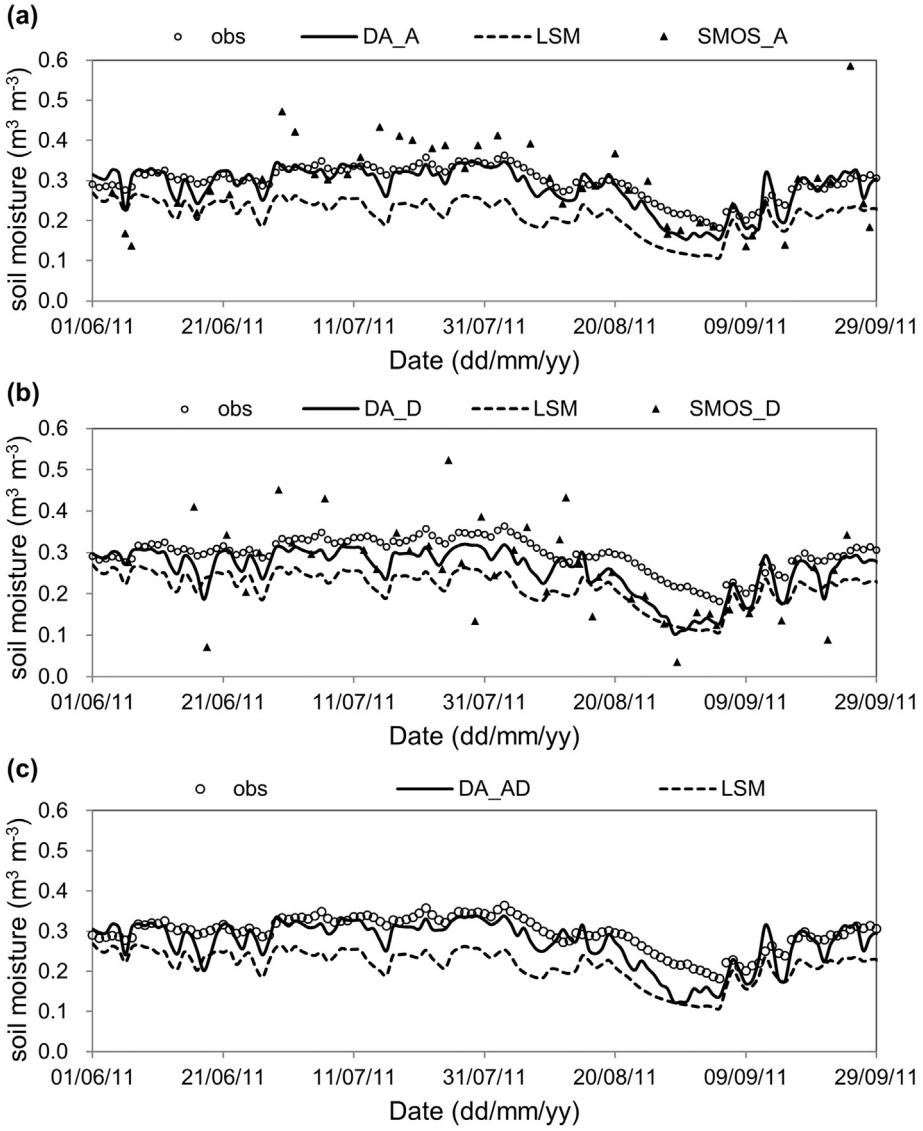

Fig. 7. Comparison of the in-situ daily SSM (obs) with the LDASUT (DA_A, DA_D, DA_AD) and LSM estimation (LSM). (a–c) Refer to the results of assimilating the ascending, descending, and both of the two passes products. SMOS_A and SMOS_D are the remote sensing retrieved SMOS L2 SSM.

Second, the L2 SSM data seem better than L3 data. L3 has more ERs than L2 during the unfrozen period, and as a consequence, more ERs in L3 than in L2 at the 100-km scale. Despite this, the L3 retrievals do not show a better accuracy than that of L2 (Fig. 6), but exhibit a larger spatial divergence (Fig. 4) and a greater temporal variation (Fig. 5), as indicated by the statistic indices in Table 1 (at the 25-km scale: RMSD > 0.200 $m^3\ m^{-3}$; at the 100-km scale: RMSD > 0.100 $m^3\ m^{-3}$). A further investigation on this degraded performance of L3 product needs to go back to the SMOS soil moisture retrieval algorithm. Yet this is beyond the scope of this study.

Table 2
Performance of different approaches in estimating SSM through LDASUT, remote sensing, and LSM. Analyzed period is from June 1, 2011 to October 1, 2011.

	Data assimilation			Remote sensing		LSM
	DA_A	DA_AD	DA_D	SMOS_A	SMOS_D	
R	0.90	0.87	0.86	0.73	0.54	0.82
BIAS	−0.012	−0.023	−0.037	−0.002	−0.035	−0.080
RMSD	0.027	0.036	0.047	0.071	0.096	0.084

Units for BIAS and RMSD: $m^3\ m^{-3}$.

As the L2 SSM data seem to have a better accuracy, it is utilized in the assimilation in Section 3.2.

Third, the diurnal cycles of soil freezing–thawing impact the performance of the retrievals. It is noteworthy that the freeze–thaw transition (see the shaded periods in Fig. 5) occurred when the ascending and descending retrievals present different biases. Both L2 and L3 ascending retrievals tend to have larger negative biases than the descending retrievals. To investigate this issue, Fig. 5e shows the observed minimum surface soil temperature of all CTP-SMTMN stations at 6:00 am (close to ascending time) and 6:00 pm (close to descending time). As aforementioned in Section 2.3, we use 0 °C as threshold to estimate the topsoil freeze–thaw status. Obviously, the minimum morning soil temperature during the shaded periods is below or equal to zero, indicating that the topsoil at one location at least was frozen, whereas the minimum evening soil temperature is always above or equal to zero, indicating the whole area was very likely unfrozen. Based on these analyses, we believe that the presence of frozen soil may have introduced uncertainties in the SMOS soil moisture retrievals. As such, a better consideration of soil freezing–thawing process is expected in the development of future retrieval algorithms.

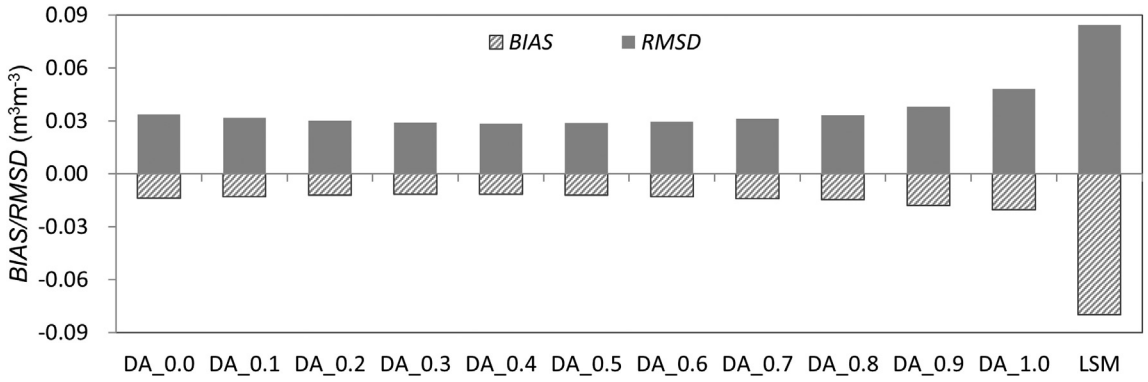

Fig. 8. Performance metrics (BIAS and RMSD) of LDASUT in estimating SSM by using different cost function forms. The number after "DA_" denotes the weight assigned to the observed error term in Eq. (2).

Last, the ascending retrieval has a better accuracy than the descending retrieval during the unfrozen period. Similar results are obtained by Dente et al. (2012) and Al-Yaari et al. (2014), in which the ascending retrieval has relative higher correlation coefficient than the descending one for either the SMOS L2 or L3 data, respectively. The ascending tends to have more ERs and behave better in capturing the SSM dynamics (Fig. 4), especially when averaged at the 100-km scale (Fig. 6). The degraded performance of the descending retrieval is very likely caused by the larger temperature gradient within the soils, as has been analyzed in detail by (Zhao, Yang, Qin, & Chen, 2013).

In a previous study, Chen et al. (2013) conducted an evaluation of four AMSR-E soil moisture products against the same dataset from this area, and found that their RMSD values range over 0.1–0.26 $m^3\ m^{-3}$. According to the evaluation, the SMOS L2 retrieval can capture the temporal change well and it performs superior to any of those AMSR-E retrievals, so the SMOS L2 soil moisture products can be recommended for further applications in the Tibetan Plateau semi-arid region. This data is also further assimilated into a land surface model to explore the optimal utilization of SMOS SSM product.

3.2. Assimilation of SMOS L2 soil moisture

The land data assimilation is implemented at a single grid (CTP-SMTMN area of 1°) and only over the unfrozen season (June 1, 2011 to October 1, 2011). The assimilated SMOS SSM is the L2 data that spatially averaged over 56 nodes within the CTP-SMTMN network area (~100 km). Three assimilation cases were conducted, including the assimilation of only ascending, only descending, and simultaneously both two overpasses of retrievals. Default SiB2 parameters were derived from several datasets. Soil thermal and hydraulic parameters and vegetation type/coverage were specified from the 1° × 1° ISLSCP (International Satellite Land Surface Climatology Project) dataset (Loveland et al., 2000; Task, 2000). Leaf area index (LAI) was originated from MODIS 0.25° × 0.25° gridded 8-day leaf area index products (Knyazikhin et al., 1999) and then interpolated to daily time series. Forcing data was obtained from the 3-hourly GLDAS-1 (the Global Land Data Assimilation System version 1) (Rodell et al., 2004) product, which was then linearly interpolated into hourly time series to match the SiB2 time step. Both the 0.25° MODIS LAI and GLDAS forcing were then spatially averaged into the 1° network area.

The daily time series of SSM estimated through three assimilation cases and open-loop land surface modeling are shown in Fig. 7. Table 2 lists the performance of different approaches, including data assimilation, remote sensing, and land surface modeling, in estimating SSM for the unfrozen season of year 2011.

The LDASUT estimate is much better than either the open-loop SiB2 simulation or remote sensing retrieving. The LSM estimate follows the trends of surface soil wetness well due to its strong response to rainfall events, but it significantly underestimates SSM (BIAS = $-0.080\ m^3\ m^{-3}$). Meanwhile, in the pure remote sensing case, the number of SMOS retrievals is not sufficient and the data contains a considerable uncertainty (RMSD > $0.070\ m^3\ m^{-3}$). Nevertheless, by assimilating the SMOS L2 soil moisture data, all the three assimilation cases greatly improve the SSM estimation with correlation coefficient over 0.85 and RMSD within $0.050\ m^3\ m^{-3}$.

Among the three assimilates cases, the assimilation of the ascending retrieval performs the best, with the highest correlation coefficient ($R = 0.90$) and the smallest error (BIAS = $-0.012\ m^3\ m^{-3}$,

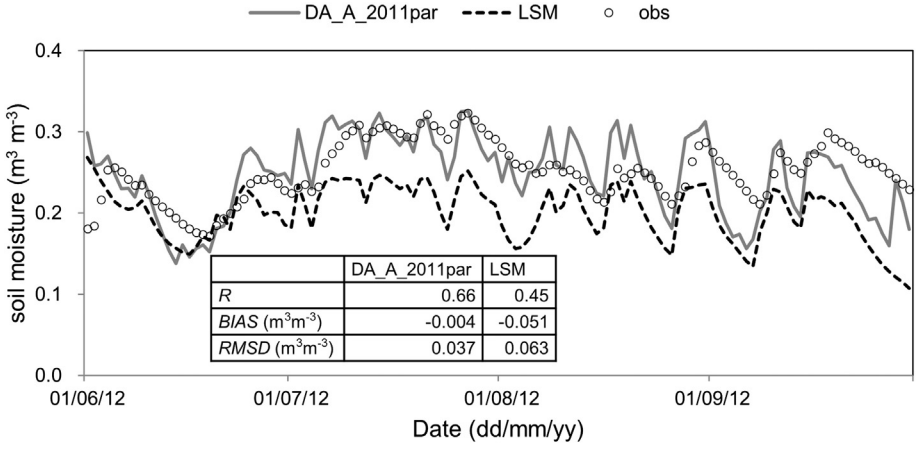

Fig. 9. Time series of daily SSM estimate based on different sets of model parameters for the unfrozen season of year 2012. LSM and DA_A_2011par refer to the use of default parameters and the ones optimized by using 2011 data, respectively. The table shows the performance of SSM estimation.

RMSD = 0.027 m^3 m^{-3}). The assimilation that merely uses the descending retrieval performs the worst among all three cases, and the joint assimilation of both retrievals shows a moderate performance. This is consistent with the fact that the descending retrieval has significant dry biases for the unfrozen season (BIAS = −0.035 m^3 m^{-3}; Table 2) as compared with the ground truth.

Although SMOS failed in providing reliable SSM through remote sensing alone, LDASUT is capable of improving the estimate with both high temporal resolution and acceptable accuracy (RMSD < 0.04 m^3 m^{-3}), by assimilating the spatially averaged SMOS retrievals into SiB2. Moreover, no extra in-situ parameter data (e.g., soil porosity) are required in the assimilation system, as they are optimized in LDASUT.

3.3. Discussions on the SMOS data assimilation

3.3.1. Sensitivity analysis to the weighting number

It is commonly recognized that both LSMs and satellite observations may have uncertainties and thus can introduce biases in soil moisture estimated within the land data assimilation system. In our assimilation, we assume SiB2 and SMOS retrievals equally contribute to the estimation error by assigning $\alpha = 0.5$ in Eq. (2). However, these two terms may have different impacts on the LDASUT output. Hence, we conduct following sensitivity analysis to justify our choice.

The assimilation time window in the sensitivity study is the same as the aforementioned assimilation cases. Fig. 8 shows the evolution of BIAS and RMSD of SSM estimated through data assimilation when α varies from 0.0 to 1.0. Clearly, no matter what value is assigned to α, all the assimilations cases outperform the open-loop run (LSM). Meanwhile, $\alpha = 0$ or $\alpha = 1.0$ will lead to larger biases. By contrast, there are only slight differences when both two sources of uncertainties are considered ($0 < \alpha < 1.0$), and the estimate reaches the best when $\alpha = 0.4$ or 0.5. Therefore, $\alpha = 0.5$ seems a reasonable choice for the regions of concern.

3.3.2. The role of parameter optimizations

Among the optimized model parameters in LDASUT, soil porosity is a key parameter to determine soil moisture content, but it is not able to be measured at a regional scale. Nevertheless, its value should be over 0.38 according to the observed in-situ SSM time series (see Fig. 5). Yet the default value of soil porosity in SiB2 is 0.31, and the optimized value based on the implementation of Pass 1 is 0.41. The latter is much higher than the former but close to the "observed" one (>0.38). Therefore, the LDASUT produces nearly unbiased SSM estimate.

To investigate the applicability of the optimized parameters, we conducted the data assimilation Pass 2 for the year of 2012, with model parameters pre-optimized (in Pass 1) in the year of 2011. Fig. 9 shows that the assimilation for 2012 produces SSM estimates very close to the observations, which is much better than the open-loop LSM simulation. This indicates that the model parameters optimized for a period may be valid for another period in the area of interest, and thus it is promising to reduce the computational load when doing the long-time data assimilation.

4. Summary

The recently launched SMOS satellite provides a magnificent opportunity to monitor the ground surface soil moisture. Various evaluations on the SMOS retrievals have been carried out worldwide, but mostly focused in Europe and America. Besides, the recently publicized SMOS L3 product is rarely evaluated. This study evaluates both SMOS L2 and L3 soil moisture products against a newly established Tibetan Plateau soil moisture network, based on which the SMOS L2 data are selected to be assimilated into a dual-pass land data assimilation system to explore the feasibility of estimating SSM with high temporal resolution and acceptable accuracy.

Both SMOS L2 and L3 products have large uncertainties at node scales, while the average over a 100-km scale can reflect the surface wetness well, and L2 data performs better than the preliminary version of L3 data. The retrievals highly depend on the climate. During the unfrozen season (June 1 to October 1), the ascending (morning) retrieval shows small biases than the descending (evening) one, perhaps due to the large temperature gradient in the evening. After averaged at the 100-km scale, the SMOS L2 ascending retrieval can approach the anticipation with RMSD = 0.060 m^3 m^{-3} during the unfrozen season. When the diurnal freezing–thawing cycle occurs, the ascending retrieval becomes degraded, due to the soil freezing in the morning. During the winter, retrievals are rarely available due to the presence of frozen soil and snow cover.

After the SMOS L2 ascending retrieval is assimilated into the dual-pass data assimilation system, the soil moisture estimate evidently outperforms the remote sensing alone or the open-loop land surface modeling. Actually, the accuracy of the estimate fulfills the expectation of the SMOS mission with RMSD ≤ 0.040 m^3 m^{-3}. This is attributed to the dual-pass framework of LDASUT that may optimize model parameters based on satellite data rather than in-situ data. Thus the SMOS L2 soil moisture assimilation scheme can be used to estimate the surface soil moisture for the Tibetan Plateau semi-arid region.

Acknowledgment

This research was financially supported by National Natural Science Foundation of China (grant nos. 41325019 and 41190083), and the National Natural Science Foundation of China (grant no. 41325019). The SMOS L3 data were obtained from the "Centre Aval de Traitement des Données SMOS" (CATDS), operated for the "Centre National d'Etudes Spatiales" (CNES, France) by IFREMER (Brest, France). GLDAS datasets are collected from the NASA Goddard Earth Sciences Data and Information Services Center (GES DISC) (http://ldas.gsfc.nasa.gov/gldas/).

References

Al Bitar, A., Leroux, D., Kerr, Y. H., Merlin, O., Richaume, P., Sahoo, A., et al. (2012). Evaluation of SMOS soil moisture products over continental U.S. using the SCAN/SNOTEL network. *IEEE Transactions on Geoscience and Remote Sensing, 50*, 1572–1586.

Albergel, C., de Rosnay, P., Gruhier, C., Muñoz-Sabater, J., Hasenauer, S., Isaksen, L., et al. (2012). Evaluation of remotely sensed and modelled soil moisture products using global ground-based in situ observations. *Remote Sensing of Environment, 118*, 215–226.

Al-Yaari, A., Wigneron, J. P., Ducharne, A., Kerr, Y., de Rosnay, P., de Jeu, R., et al. (2014). Global-scale evaluation of two satellite-based passive microwave soil moisture datasets (SMOS and AMSR-E) with respect to Land Data Assimilation System estimates. *Remote Sensing of Environment, 149*, 181–195.

Bartalis, Z., Wagner, W., Naeimi, V., Hasenauer, S., Scipal, K., Bonekamp, H., et al. (2007). Initial soil moisture retrievals from the METOP-A Advanced Scatterometer (ASCAT). *Geophysical Research Letters, 34* (L20401).

Chen, Y., Yang, K., Qin, J., Zhao, L., Tang, W., & Han, M. (2013). Evaluation of AMSR-E retrievals and GLDAS simulations against observations of a soil moisture network on the central Tibetan Plateau. *Journal of Geophysical Research - Atmospheres, 118*, 4466–4475.

Crow, W. T., Berg, A. A., Cosh, M. H., Loew, A., Mohanty, B. P., Panciera, R., et al. (2012). Upscaling sparse ground-based soil moisture observations for the validation of coarse-resolution satellite soil moisture products. *Reviews of Geophysics, 50* (RG2002).

Crow, W. T., & Wood, E. F. (2003). The assimilation of remotely sensed soil brightness temperature imagery into a land surface model using Ensemble Kalman filtering: A case study based on ESTAR measurements during SGP97. *Advances in Water Resources, 26*, 137–149.

dall'Amico, J. T., Schlenz, F., Loew, A., & Mauser, W. (2012). First results of SMOS soil moisture validation in the upper Danube catchment. *IEEE Transactions on Geoscience and Remote Sensing, 50*, 1507–1516.

Dente, L., Su, Z., & Wen, J. (2012). Validation of SMOS soil moisture products over the Maqu and Twente regions. *Sensors, 12*, 9965–9986.

Dorigo, W. A., Wagner, W., Hohensinn, R., Hahn, S., Paulik, C., Xaver, A., et al. (2011). The International Soil Moisture Network: A data hosting facility for global in situ soil moisture measurements. *Hydrology and Earth System Sciences, 15*, 1675–1698.

Duan, Q. Y., Gupta, V. K., & Sorooshian, S. (1993). Shuffled complex evolution approach for effective and efficient global minimization. *Journal of Optimization Theory and Applications, 76*, 501–521.

Entin, J., Robock, A., Vinnikov, K. Y., Zabelin, V., Liu, S., Namkhai, A., et al. (1999). Evaluation of global soil wetness project soil moisture simulations. *Journal of the Meteorological Society of Japan*, *77*, 183–198.

Gherboudj, I., Magagi, R., Goita, K., Berg, A. A., Toth, B., & Walker, A. (2012). Validation of SMOS data over agricultural and boreal forest areas in Canada. *IEEE Transactions on Geoscience and Remote Sensing*, *50*, 1623–1635.

Hall, D. K., Salomonson, V. V., & Riggs, G. A. (2006a). *MODIS/Aqua Snow Cover Daily L3 Global 0.05Deg CMG. Version 5. August 2010 to November 2012.* Boulder, Colorado USA: National Snow and Ice Data Center.

Hall, D. K., Salomonson, V. V., & Riggs, G. A. (2006b). *MODIS/Terra Snow Cover Daily L3 Global 0.05Deg CMG. Version 5. August 2010 to November 2012.* Boulder, Colorado, USA: National Snow and Ice Data Center.

Henderson-Sellers, A., Yang, Z. L., & Dickinson, R. E. (1993). The project for intercomparison of land-surface parameterization schemes. *Bulletin of the American Meteorological Society*, *74*, 1335–1349.

Houser, P. R., Shuttleworth, W. J., Famiglietti, J. S., Gupta, H. V., Syed, K. H., & Goodrich, D. C. (1998). Integration of soil moisture remote sensing and hydrologic modeling using data assimilation. *Water Resources Research*, *34*, 3405–3420.

Jackson, T. J., Bindlish, R., Cosh, M. H., Tianjie, Z., Starks, P. J., Bosch, D.D., et al. (2012). Validation of soil moisture and ocean salinity (SMOS) soil moisture over watershed networks in the U.S. *IEEE Transactions on Geoscience and Remote Sensing*, *50*, 1530–1543.

Kerr, Y., Jacquette, E., Al Bitar, A., Cabot, F., Mialon, A., Richaume, P., et al. (2013). *CATDS SMOS L3 Soil moisture retrieval processor ATBD.* CESBIO and CNES, SO-TN-CBSA-GS-0029.

Kerr, Y., Waldteufel, P., Richaume, P., Davenport, I., Ferrazzoli, P., & Wigneron, J. -P. (2010a). *SMOS Level 2 Processor Soil Moisture ATBD.* SM-ESL (CBSA), Toulouse SO-TN-ESL-SM-GS-0001.

Kerr, Y. H., Waldteufel, P., Richaume, P., Wigneron, J. P., Ferrazzoli, P., Mahmoodi, A., et al. (2012). The SMOS soil moisture retrieval algorithm. *IEEE Transactions on Geoscience and Remote Sensing*, *50*, 1384–1403.

Kerr, Y. H., Waldteufel, P., Wigneron, J. P., Delwart, S., Cabot, F., Boutin, J., et al. (2010b). The SMOS mission: New tool for monitoring key elements ofthe global water cycle. *Proceedings of the IEEE*, *98*, 666–687.

Kerr, Y. H., Waldteufel, P., Wigneron, J. -P., Martinuzzi, J., Font, J., & Berger, M. (2001). Soil moisture retrieval from space: The Soil Moisture and Ocean Salinity (SMOS) mission. *IEEE Transactions on Geoscience and Remote Sensing*, *39*, 1729–1735.

Knyazikhin, Y., Glassy, J., Privette, J., Tian, Y., Lotsch, A., Zhang, Y., et al. (1999). *MODIS leaf area index (LAI) and fraction of photosynthetically active radiation absorbed by vegetation (FPAR) product (MOD15) algorithm theoretical basis document.* Theoretical Basis Document. Greenbelt, MD: NASA Goddard Space Flight Center.

Koike, T., Nakamura, Y., Kaihotsu, I., Davva, G., Matsuura, N., Tamagawa, K., et al. (2004). Development of an advanced microwave scanning radiometer (AMSR-E) algorithm of soil moisture and vegetation water content. *Annual Journal of Hydraulic Engineering, JSCE*, *48*, 217–222.

Koster, R. D., Dirmeyer, P. A., Guo, Z. C., Bonan, G., Chan, E., Cox, P., et al. (2004). Regions of strong coupling between soil moisture and precipitation. *Science*, *305*, 1138–1140.

Li, X., Huang, C., Che, T., Jin, R., Wang, S., Wang, J., et al. (2007). Development of a Chinese land data assimilation system: Its progress and prospects. *Progress in Natural Science*, *17*, 881–892.

Loveland, T. R., Reed, B. C., Brown, J. F., Ohlen, D. O., Zhu, Z., Yang, L., et al. (2000). Development of a global land cover characteristics database and IGBP DISCover from 1 km AVHRR data. *International Journal of Remote Sensing*, *21*, 1303–1330.

Margulis, S. A., McLaughlin, D., Entekhabi, D., & Dunne, S. (2002). Land data assimilation and estimation of soil moisture using measurements from the Southern Great Plains 1997 Field Experiment. *Water Resources Research*, *38*, 1299.

McMullan, K. D., Brown, M.A., Martin-Neira, M., Rits, W., Ekholm, S., Marti, J., et al. (2008). SMOS: The payload. *IEEE Transactions on Geoscience and Remote Sensing*, *46*, 594–605.

Montzka, C., Moradkhani, H., Weihermuller, L., Franssen, H. J. H., Canty, M., & Vereecken, H. (2011). Hydraulic parameter estimation by remotely-sensed top soil moisture observations with the particle filter. *Journal of Hydrology*, *399*, 410–421.

Moradkhani, H., Sorooshian, S., Gupta, H. V., & Houser, P. R. (2005). Dual state-parameter estimation of hydrological models using ensemble Kalman filter. *Advances in Water Resources*, *28*, 135–147.

Njoku, E. G., & Chan, S. K. (2006). Vegetation and surface roughness effects on AMSR-E land observations. *Remote Sensing of Environment*, *100*, 190–199.

Njoku, E. G., & Entekhabi, D. (1996). Passive microwave remote sensing of soil moisture. *Journal of Hydrology*, *184*, 101–129.

Njoku, E. G., Jackson, T. J., Lakshmi, V., Chan, T. K., & Nghiem, S. V. (2003). Soil moisture retrieval from AMSR-E. *IEEE Transactions on Geoscience and Remote Sensing*, *41*, 215–229.

Oliva, R., Daganzo, E., Kerr, Y. H., Mecklenburg, S., Nieto, S., Richaume, P., et al. (2012). SMOS radio frequency interference scenario: Status and actions taken to improve the RFI environment in the 1400–1427-MHz passive band. *IEEE Transactions on Geoscience and Remote Sensing*, *50*, 1427–1439.

Owe, M., de Jeu, R., & Holmes, T. (2008). Multisensor historical climatology of satellite-derived global land surface moisture. *Journal of Geophysical Research, Earth Surface*, *113* F01002.

Pan, M., Sahoo, A. K., Wood, E. F., Al Bitar, A., Leroux, D., & Kerr, Y. H. (2012). An initial assessment of SMOS derived soil moisture over the continental United States. *IEEE Journal of Selected Topics in Applied Earth Observations and Remote Sensing*, *5*, 1448–1457.

Pan, M., & Wood, E. F. (2006). Data assimilation for estimating the terrestrial water budget using a constrained ensemble kalman filter. *Journal of Hydrometeorology*, *7*, 534–547.

Qin, J., Liang, S. L., Yang, K., Kaihotsu, I., Liu, R. G., & Koike, T. (2009). Simultaneous estimation of both soil moisture and model parameters using particle filtering method through the assimilation of microwave signal. *Journal of Geophysical Research-Atmospheres*, *114* D15103.

Qin, J., Yang, K., Lu, N., Chen, Y. Y., Zhao, L., & Han, M. L. (2013). Spatial upscaling of in-situ soil moisture measurements based on MODIS-derived apparent thermal inertia. *Remote Sensing of Environment*, *138*, 1–9.

Reichle, R. H., Crow, W. T., & Keppenne, C. L. (2008). An adaptive ensemble Kalman filter for soil moisture data assimilation. *Water Resources Research*, *44* W03423.

Rodell, M., Houser, P. R., Jambor, U., Gottschalck, J., Mitchell, K., Meng, C. J., et al. (2004). The global land data assimilation system. *Bulletin of the American Meteorological Society*, *85*, 381–394.

Rowlandson, T. L., Hornbuckle, B. K., Bramer, L. M., Patton, J. C., & Logsdon, S. D. (2012). Comparisons of evening and morning SMOS passes over the midwest United States. *IEEE Transactions on Geoscience and Remote Sensing*, *50*, 1544–1555.

Sabater, J. M., Fouilloux, A., & de Rosnay, P. (2011). Technical implementation of SMOS data in the ECMWF integrated forecasting system. *IEEE Geoscience and Remote Sensing Letters*, *9*, 252–256.

Sanchez, N., Martinez-Fernandez, J., Scaini, A., & Perez-Gutierrez, C. (2012). Validation of the SMOS L2 Soil Moisture Data in the REMEDHUS Network (Spain). *IEEE Transactions on Geoscience and Remote Sensing*, *50*, 1602–1611.

Schmugge, T. (1978). Remote sensing of surface soil moisture. *Journal of Applied Meteorology*, *17*, 1549–1557.

Sellers, P. J., Randall, D. A., Collatz, G. J., Berry, J. A., Field, C. B., Dazlich, D. A., et al. (1996). A revised land surface parameterization (SiB2) for atmospheric GCMs .1. Model formulation. *Journal of Climate*, *9*, 676–705.

Su, Z., Wen, J., Dente, L., van der Velde, R., Wang, L., Ma, Y., et al. (2011). The Tibetan Plateau observatory of plateau scale soil moisture and soil temperature (Tibet-Obs) for quantifying uncertainties in coarse resolution satellite and model products. *Hydrology and Earth System Sciences*, *15*, 2303–2316.

Task, G. S. D. (2000). Global Soil Data Products CD-ROM (IGBP-DIS). International Geosphere-Biosphere Programme-Data and Information Available Services. Available online at http://www.daac.ornl.gov.

Tian, X. J., Xie, Z. H., Dai, A., Shi, C. X., Jia, B. H., Chen, F., et al. (2009). A dual-pass variational data assimilation framework for estimating soil moisture profiles from AMSR-E microwave brightness temperature. *Journal of Geophysical Research-Atmospheres*, *114*.

Wigneron, J. P., Kerr, Y., Waldteufel, P., Saleh, K., Escorihuela, M. J., Richaume, P., et al. (2007). L-band microwave emission of the biosphere (L-MEB) model: Description and calibration against experimental data sets over crop fields. *Remote Sensing of Environment*, *107*, 639–655.

Yang, K., Qin, J., Zhao, L., Chen, Y., Tang, W., Han, M., et al. (2013). A multi-scale soil moisture and freeze–thaw monitoring network on the third pole. *Bulletin of the American Meteorological Society*, *94*, 1907–1916.

Yang, K., Watanabe, T., Koike, T., Li, X., Fuji, H., Tamagawa, K., et al. (2007). Auto-calibration system developed to assimilate AMSR-E data into a land surface model for estimating soil moisture and the surface energy budget. *Journal of the Meteorological Society of Japan*, *85A*, 229–242.

Young, P. C. (2002). Advances in real-time flood forecasting. *Philosophical Transactions of the Royal Society of London Series A*, *360*, 1433–1450.

Zhao, L., Yang, K., Qin, J., & Chen, Y. (2013a). Optimal exploitation of AMSR-E signals for improving soil moisture estimation through land data assimilation. *IEEE Transactions on Geoscience and Remote Sensing*, *51*, 399–410.

Zhao, L., Yang, K., Qin, J., Chen, Y., Tang, W., Montzka, C., et al. (2013b). Spatiotemporal analysis of soil moisture observations within a Tibetan mesoscale area and its implication to regional soil moisture measurements. *Journal of Hydrology*, *482*, 92–104.